Atomic Force Microscopy Investigations of Collagen: From Single Molecules to Fibrils

Janine Srocka*[1], Alaa Al-Shaer*[1] and Nancy R. Forde[†2]

[1]Department of Molecular Biology and Biochemistry, Simon Fraser University

[2]Department of Physics, Simon Fraser University

*Equal contributions

[†]Corresponding author: nforde@sfu.ca

Running head: AFM imaging and analysis of collagen

Abstract

Collagen is a key component of the extracellular matrix, providing structural support and influencing cellular behaviour through its physical properties. Understanding its mechanical properties is essential for elucidating its role in tissue integrity and pathology. Collagen forms complex hierarchical structures, ranging from individual proteins to higher-order fibrils, fibers, and networks, each contributing to the mechanical stability of tissues. In this methods chapter we outline the use of atomic force microscopy (AFM) to investigate collagen's structural properties across multiple hierarchical levels, from single molecules to fibrils. We describe the preparation of collagen samples for AFM analysis of collagen in three forms: proteins, reconstituted fibrils, and tendon-derived fibrils from rat tails. Additionally, we describe a MATLAB-based image analysis method for quantitatively assessing mechanical properties of individual collagen proteins.

Keywords: Collagen, Atomic Force Microscopy (AFM), Single-Molecule Imaging, Fibrils, Mechanics, Protein Structure, Image Analysis, Persistence Length

1 Introduction

Collagen is an integral component of the extracellular matrix, providing structural support to tissues. This role is vividly demonstrated in decellularized organs, where tissues retain their architectural integrity even in the absence of cells [1]. Over the years, our understanding of collagen has evolved beyond its function as simply a physical framework. We now recognize it as a dynamic scaffold that influences cellular behaviour through its physical properties [2]. As tissues are dynamic structures constantly subjected to mechanical loads, collagen is crucial in maintaining mechanical integrity, enabling tissues to endure mechanical stresses and uphold homeostasis [3].

The collagen protein can assemble to form diverse higher-order structures ranging from fibrils to fibres and networks [4,5]. The smallest functional unit is the individual protein composed of three left-handed proline-rich polypeptide α-chains, which assemble into a right-handed triple helix of approximately 300 nm in length (for fibril-forming collagens) and 1.5 nm in diameter [4,6]. Each chain consists of a repetitive Gly-X-Y sequence, where X and Y can be any amino acid but are often proline and hydroxyproline, respectively [4,5]. There are 28 unique types of collagen, of which fibril-forming collagens are the most abundant [4]. In tendons, collagen fibrils are highly organized assemblies primarily composed of type I collagen proteins. These fibrils can reach diameters of several hundred nanometers and lengths extending up to millimeters [7-9]. Proteins within these fibrils align laterally, staggered by 67 nm along their long axis, creating a characteristic banded structure (“D-banding”) of alternating regions with higher (overlap region) and lower (gap region) protein density. Five adjacent proteins form a right-handed helical microfibril, which interdigitates with neighbouring microfibrils to form a long cylindrical

layered fibril [10]. The stability of these assemblies is reinforced by crosslink formation between individual collagen proteins within a fibril [11]. Multiple fibrils can then assemble to form fibers, which can further combine to create higher-order structures in tendons called fascicles [12].

Studying collagen proteins in their full-length form presents significant challenges due to their large size (≥300 kDa, ≥300 nm in length) and tendency to self-organize into non-crystalline structures, which limits the application of conventional structural analysis techniques. The structure of fibrils has been analysed with X-ray diffraction [10,13], though not reaching atomic resolution, while short peptides (~30 amino acids, ~10 nm) are more suitable for high-resolution studies using crystallization and NMR analyses [14,15].

Atomic force microscopy (AFM) imaging offers an alternative approach that is capable of exploring collagen's structural properties across different hierarchical levels, from individual proteins to higher-order structures like fibrils. AFM generates detailed nanoscale topographic maps, providing comprehensive 3D surface profiles with the potential for atomic resolution, making it a powerful tool for investigating materials across a wide range of scales [16,17]. Unlike electron microscopy, which often requires heavy-metal treatment of biological samples, AFM offers a non-invasive approach with minimal sample preparation, preserving the integrity of delicate specimens and their intrinsic material properties and allowing for investigations close to native conditions [18].

While we have seen much progress being made in understanding how post-translational modifications, cross-linking, tissue origin, and strain type influence the mechanical properties of collagen fibrils [19], the impact of chemical changes on mechanics at the individual protein level

remains less well understood [6]. Alterations in collagen's composition are associated with a variety of diseases, including osteogenesis imperfecta and Ehlers-Danlos syndrome [20], and physiological dysfunction can arise from alterations due to aging-related nonenzymatic glycation or post-translational modifications [4,21,22]. These chemical changes at the protein level are associated with altered tissue structure and mechanics in disease [23,24]. Given collagen's hierarchical structure, understanding how chemical changes affect tissue mechanics requires an in-depth examination of how these modifications influence mechanics at the molecular level.

In this methods chapter, we describe the use of AFM to visualize collagen's structure at different hierarchical levels. We outline the preparation of the following three distinct forms of collagen for AFM analysis: individual proteins, reconstituted fibrils, and tendon-derived fibrils from rat tails. This chapter focuses on the preparation of collagen samples for AFM imaging; we assume the reader to have access to an AFM for which operational support is available to perform sample imaging. References [25-27] provide descriptions of using AFM to image biological samples. In this chapter, we also provide an overview of how to use a MATLAB-based quantitative image analysis method, SmarTrace, to assess mechanical properties of single molecules like individual collagen proteins. To learn more about how AFM imaging and SmarTrace can be implemented to better understand collagen mechanics at the molecular level, we refer the interested reader to the following applications of AFM imaging by our research group: characterizing the mechanical properties of collagens type I, II and III in different ionic and pH conditions [28,29], mapping how the bending stiffness of types III and IV collagen depends on their local sequence [30], investigating the thermally induced

denaturation and refolding pathways of type IV collagen [31], and studying the effects of post-translational enzymatic modifications [32] and Age-related Glycation End-products (AGEs) on the flexibility of collagen I [33]. At the fibril level, AFM can be used to study various properties of collagen fibrils such as quantifying D-banding periodicity [34,35], electrostatic mapping of surfaces via Kelvin Probe Microscopy [36-38], and mechanics via nanoindentation and other approaches [39-45]. Time-lapse and high-speed AFM imaging are also beginning to reveal the mechanism of collagen self-assembly [46-48], opening up new approaches to understanding how these proteins form diverse higher-order structures whose mechanics are vital to physiological function.

2 Materials

2.1 Proteins and Reconstituted Fibrils

- Rat-tail Collagen Type I (Cultrex®, 3440-100-01)
- Mica (Highest Grade V1 AFM Mica Discs, 10 mm; Ted Pella, Redding, CA)
- Metal plate (AFM Specimen Discs, 12 mm, Ted Pella, Redding, CA)
- Double-sided tape (Nonconductive Double Sided Adhesive Discs, 10 mm, SPI Supplies, West Chester, PA)
- Tape (Scotch® Magic™ Tape 12 mm, 3M, Saint Paul, MN)
- ddH_2O
- Desired solution for imaging collagen proteins (e.g. 100 mM KCl, 1 mM HCl)
- 10X fibril-forming buffer: 2.73 M NaCl, 50 mM KCl, 420 mM Na_2HPO_4 and 90 mM KH_2PO_4, pH 7

- Compressed air filter (Millipak® 40 Sterile, MilliporeSigma, Burlington, MA, depicted in Figure 4, Step 11)
- AFM tip recommendation: 160-kHz resonance frequency and 5 N/m force constant (e.g. MikroMasch, HQ: NSC14/AL BS; Sofia, Bulgaria)

2.2 Native Fibrils Extracted from Tendon

- Rat tail
- Glass coverslip
- Surgical Scissors
- Sharp Tweezers
- ddH_2O
- 1X PBS pH 7.4, e.g. prepared from 10X PBS (Phosphate Buffered Saline 10X solution, BP3994, Fisher BioReagents™)
- Compressed air filter (Millipak® 40 Sterile, MilliporeSigma, Burlington, MA, depicted in Figure 4, Step 11)
- AFM tip recommendation: 160-kHz resonance frequency and 5 N/m force constant (e.g. MikroMasch, HQ: NSC14/AL BS; Sofia, Bulgaria)

3 Methods

3.1 Proteins and Reconstituted Fibrils

3.1.1 AFM Sample Preparation

1. Attach a mica disk to a metal plate using double-sided tape.
2. Place a heavy object on top to firmly flatten the mica disk and ensure strong adhesion.
3. Apply regular Scotch tape to the mica surface and quickly peel it off, pulling perpendicularly to the plate, to peel of a layer of mica and expose a fresh mica surface.

Sample Preparation for Imaging and Analysis of Individual Collagen Proteins

4. Dilute collagen into a desired solution to achieve a final concentration of approximately 0.1 μg/mL of collagen proteins.
5. Deposit 50 μL of the diluted collagen sample onto the freshly cleaved mica surface, and allow the sample to sit for 10–30 seconds to facilitate adsorption.
6. Remove salts and excess unbound proteins by rinsing the mica gently with 0.5–1 mL ultrapure water.
7. Dry the mica surface completely using filtered air. The sample is now prepared for AFM imaging in air. An example image of single collagen molecules can be seen in Figure 1.

Sample Preparation for Imaging and Analysis of Reconstituted Collagen Fibrils

4. Dilute acid-soluble collagen to a final concentration of 0.1–1 mg/mL in 1X fibril-forming buffer.
5. Allow collagen to assemble into fibrils for at least one hour at the appropriate temperature (typically 25–35°C). The sample should form a gel with visible white, stringy structures. *Optional:* Monitor the kinetics of collagen fibril formation by the increasing turbidity / optical density at 347 nm as fibrils assemble [49,34].

6. Deposit 50 µL of the assembled collagen sample onto the freshly cleaved mica surface and allow the sample to air dry completely to facilitate the adsorption of larger fibrillar structures.
7. Gently rinse the mica with 0.5–1 mL ultrapure water to remove salts and unbound proteins.
8. Dry the mica surface completely using filtered air. The sample is now prepared for AFM imaging in air. An example image of reconstituted fibrils can be seen in Figure 1.

3.1.2 Single-Molecule Tracing and Analysis

AFM images of collagen proteins can be analysed to obtain information on mechanical properties including persistence length/bending stiffness and curvature [28]. To do so, we developed software in MATLAB called SmarTrace that can trace the backbones of collagen proteins and analyse the statistical distributions of the bends in these proteins to provide persistence length and curvature of collagen under varying conditions of deposition on the mica [28,50]. Here, we provide an overview of the program and how to use it.

SmarTrace analyzes polymers by tracing images of their contours to extract coordinates, enabling the application of polymer physics tools to determine physical properties [51]. Starting with a few user-defined inputs for each chain, the program refines the initial trace to identify the backbone contour and generate chain coordinates. (An automated version of this software, AutoSmarTrace, can also be used, in cases when the entire chain's backbone is not needed for mechanical analysis [29].) Backbone chain coordinates enable conformational analysis, such as calculating tangent vectors and their decorrelation, or the mean squared end-to-end distance,

to estimate structural properties such as the persistence length, a mechanical property that quantifies bending flexibility. Refer to Table 1 for detailed information on the parameters and equations used in the worm-like chain (WLC) model to extract properties of filamentous structures (modelled as polymers) such as collagen. Previous work in our group demonstrated that the ionic strength of deposition conditions influences the curvature of collagen on mica [28]. To account for this, a curved WLC (cWLC) model was derived, in which the lowest-energy conformation of the polymer is curved, as opposed to the straight rod conformation assumed by the standard WLC model [28]. The cWLC model is also incorporated as a fitting option in SmarTrace (Fig. 3). To obtain sequence-dependent information, collagen can be treated as a heterogeneous polymer using a sliding window approach to calculate persistence length over a short segment of the chain [30].

1. Download the **SmarTrace** folder and the **DIPimage** zip folder from the Forde Lab repository on GitHub [52,53].
2. Open the file SmarTrace.m located in the folder 'C:\...\SmarTrace\SmarTrace\ChainTracing'.
3. Set the **Current Folder** in MATLAB to the folder containing the images.
4. Add the DIPimage toolbox to the MATLAB workspace by entering >>addpath('C:\...\DIPimage 2.8\common\dipimage') in the Command Window, using the location of the dipimage folder on your system.
5. Initialize DIPimage by entering >>dip_initialise into the Command Window.
6. Click **Run** under the **Editor** tab in MATLAB to open the SmarTrace GUI window (Figure 2).

7. Click **Select Height Map** in the top-right corner to load an image.
8. Enter the image resolution in nanometers per pixel (nm/px). For example, for an image size of 2000 nm x 2000 nm that is 512 pixels x 512 pixels, enter 3.906 nm/px.
9. Click **Select Chain**, then use the cursor to define a few points on the chain you want to trace, ideally marking the start and end points (see Figure 2 Initial Selection panel).
10. Use the following keyboard shortcuts to refine the trace:
    - Press **Z** to zoom into the chain.
    - Press **A** to zoom out.
    - Press **D** to delete unwanted points and retrace with better precision.
11. After manually tracing the chain, press **Enter**. SmarTrace will process the chain and plot a red curve along it. The contour length (labelled 'arclen' in the Command Window) will be displayed in the MATLAB Command Window.
12. If satisfied with the traced chain:
    - Click **Add Chain** to save the chain data.
    - Click **+** to increment the chain number for tracking.
13. Repeat steps 9-12 for additional chains. To analyze chains from a new image, load a new height map before selecting **Select Chain**.
14. Save the results using **Save Image** for traced images and **Save Data** (.mat) for chain data. To continue adding chains to the data set, click **Reload Data** to load the saved file and resume tracing. The saved .mat file is used for statistical analysis of chain properties.
15. To analyze the data, open the analyseMOD.m file and type the following in the Command Window >>analyseMOD(input,output,LowerLimit,exclude,ko)

- input: The saved .mat file containing the chain coordinates.
- output: The name of the output folder for the analysis.
- LowerLimit: Ideally set to 10, specifying the bin size for length increments (nm).
- exclude: Set to 0 to include all chains; otherwise, specify indices of chains to remove.
- ko: Set to 0 for the standard WLC model or 1 for the curved WLC model [28].

16. Open the output folder to view the results, which include $\langle cos\ \theta(s) \rangle$ and $\langle R^2(s) \rangle$ values determined at segment lengths ranging from 10 nm to 200 nm in 10 nm intervals, and the respective fits to the WLC model (example fits shown in Figure 3) [28]. The .csv file contains the value for persistence length for each segment length range (the value obtained for the largest range, up to 200 nm, is typically reported), along with the associated standard error, goodness of fit (gof), and Akaike Information Criterion (AIC) statistical measures.

3.2 Native Fibrils Extracted from Tendon

Each of the following steps is depicted in Figure 4.

1. Using a pair of surgical scissors, cut the skin along the dorsal side of the rat tail (opposite the large blood vessel) from the proximal end to the distal end.

2. Carefully start to peel the skin away from the proximal towards the distal end using a pair of tweezers, to expose the underlying white tendon.
3. With the surgical scissors, cut the tendon a few centimetres away from the proximal end and pull out individual fascicles by grabbing them at the cutting site with tweezers.
4. Rinse the extracted fascicle piece with PBS. (For long-term storage, fascicles can be kept in PBS with 20% DMSO at -20 °C.)
5. Gently stretch the fascicle piece along on a glass surface and add a few drops of PBS to ensure full coverage of the fascicle with liquid.
6. Using sharp tweezers, gently fray one end of the fascicle piece, by either pulling the end apart with two pairs of tweezers or gently pressing down on the end and sliding the tweezers across the fascicle piece.
7. Grab the fascicle piece at the other end with the tweezers, transfer it to a fresh glass coverslip, and splay out the frayed end into a fan shape.
8. Grab the unfrayed end with the tweezers and slowly drag the fascicle across the coverslip surface.
9. Repeat steps 7 and 8, placing the fascicle piece at different locations on the glass coverslip until a sufficient amount of the surface has been covered. (Fibrils will appear as a slightly milky smear, like glue residue.)
10. Rinse the coverslip with ultrapure water to remove loosely bound fibrils.
11. Dry the glass surface completely using filtered air. The sample is now prepared for AFM imaging in air. An example AFM image of tendon-extracted collagen fibrils can be seen in Figure 1.

4 Notes

- Collagen can be deposited under different buffer conditions. However strong alignment of collagen with the mica lattice can be seen for a variety of neutral pH buffers such as PBS and HEPES, which therefore shouldn't be used if extraction of mechanical information is desired.
- The optimal collagen concentration for protein deposition can vary under different buffer conditions. Deposition in MES buffer for example is very slow and would require a significantly increased collagen concentration and/or incubation time.
- For deposition of collagen proteins, we recommend preparing a fresh dilution directly before deposition, since collagen tends to adhere to the tube surface over time, which will decrease the collagen content of the solution.
- Collagen fibrils can be formed in a variety of buffers of different ionic strengths and pH [54-56]. We have successfully reconstituted fibrils in the fibril-forming buffer described here [49,34], in PBS [57,58,33] and in HEPES [59].
- To pipette collagen fibrils without disrupting their structure, use scissors to cut the pipette tip and enlarge the opening. This reduces shear forces when pipetting.
- When reconstituted collagen fibrils are deposited onto mica and air-dried, regions of the mica may appear less reflective (fibrils leave a residue). When searching for fibrils with AFM, try to image over these less reflective regions.
- For obtaining images suitable for SmarTrace analysis, we usually scan 2x2 µm images with 512x512 pixels^2 and save them as a .tiff file.

- AFM images may be flattened to remove imaging artifacts before uploading them into SmarTrace, however, this is not a requirement.
- Before starting the SmarTrace analysis, ensure the following MATLAB toolboxes are installed:
    - Deep Learning Toolbox
    - Curve Fitting Toolbox
    - Computer Vision Toolbox
    - Signal Processing Toolbox
    - Statistics and Machine Learning Toolbox
    - Image Processing Toolbox

      These toolboxes can be added during MATLAB installation or later by going to the **Home** tab, clicking on **Add-Ons**, and searching for the required toolboxes
- Issues with tracing will arise if a new image is selected in the SmarTrace GUI using the "Select Height Map" button while the "Select Chain" button has already been clicked. To resolve, trace a chain and press Enter to display the refined spline. ("Select Chain" will no longer be active.) Then, go to "Select Height Map" and select the new image.
- If a region with high pixel intensity (such as debris) is located near the chain of interest, select points further away from this area to guide the refined trace away from the unwanted region.

Acknowledgements

This work was supported by a Discovery Grant from the Natural Sciences and Engineering Research Council of Canada (NSERC) to NRF. The authors thank Daniel Sloseris for tracing collagen chains for the analysis shown in Fig. 3A.

References

1. Moffat D, Ye K, Jin S (2022) Decellularization for the retention of tissue niches. Journal of Tissue Engineering 13:20417314221101151. doi:10.1177/20417314221101151

2. Pozzi A, Yurchenco PD, Iozzo RV (2017) The nature and biology of basement membranes. Matrix Biology 57-58:1-11. doi:https://doi.org/10.1016/j.matbio.2016.12.009

3. Humphrey JD, Dufresne ER, Schwartz MA (2014) Mechanotransduction and extracellular matrix homeostasis. Nature Reviews Molecular Cell Biology 15 (12):802-812. doi:10.1038/nrm3896

4. Shoulders MD, Raines RT (2009) Collagen Structure and Stability. Annual Review of Biochemistry 78 (Volume 78, 2009):929-958. doi:https://doi.org/10.1146/annurev.biochem.77.032207.120833

5. Fidler AL, Boudko SP, Rokas A, Hudson BG (2018) The triple helix of collagens – an ancient protein structure that enabled animal multicellularity and tissue evolution. Journal of Cell Science 131 (7). doi:10.1242/jcs.203950

6. Kirkness MWH, Lehmann K, Forde NR (2019) Mechanics and structural stability of the collagen triple helix. Current Opinion in Chemical Biology 53:98-105. doi:https://doi.org/10.1016/j.cbpa.2019.08.001

7. Parry DAD, Barnes GRG, Craig AS, Phillips DC (1978) A comparison of the size distribution of collagen fibrils in connective tissues as a function of age and a possible relation between fibril size distribution and mechanical properties. Proceedings of the Royal Society of London Series B Biological Sciences 203 (1152):305-321. doi:doi:10.1098/rspb.1978.0107

8. Starborg T, Kalson NS, Lu Y, Mironov A, Cootes TF, Holmes DF, Kadler KE (2013) Using transmission electron microscopy and 3View to determine collagen fibril size and three-dimensional organization. Nature Protocols 8 (7):1433-1448. doi:10.1038/nprot.2013.086

9. Svensson RB, Herchenhan A, Starborg T, Larsen M, Kadler KE, Qvortrup K, Magnusson SP (2017) Evidence of structurally continuous collagen fibrils in tendons. Acta Biomaterialia 50:293-301. doi:https://doi.org/10.1016/j.actbio.2017.01.006

10. Orgel JPRO, Irving TC, Miller A, Wess TJ (2006) Microfibrillar structure of type I collagen in situ. Proceedings of the National Academy of Sciences 103 (24):9001-9005. doi:doi:10.1073/pnas.0502718103

11. Avery NC, Bailey AJ (2008) Restraining Cross-Links Responsible for the Mechanical Properties of Collagen Fibers: Natural and Artificial. In: Fratzl P (ed) Collagen: Structure and Mechanics. Springer US, Boston, MA, pp 81-110. doi:10.1007/978-0-387-73906-9_4

12. Zhang S, Ju W, Chen X, Zhao Y, Feng L, Yin Z, Chen X (2022) Hierarchical ultrastructure: An overview of what is known about tendons and future perspective for tendon engineering. Bioactive Materials 8:124-139. doi:https://doi.org/10.1016/j.bioactmat.2021.06.007

13. Antipova O, Orgel JPRO (2010) In Situ D-periodic Molecular Structure of Type II Collagen. Journal of Biological Chemistry 285 (10):7087-7096. doi:10.1074/jbc.M109.060400

14. Bella J, Eaton M, Brodsky B, Berman HM (1994) Crystal and Molecular Structure of a Collagen-Like Peptide at 1.9 Å Resolution. Science 266 (5182):75-81. doi:doi:10.1126/science.7695699

15. Bella J (2016) Collagen structure: new tricks from a very old dog. Biochemical Journal 473 (8):1001-1025. doi:10.1042/bj20151169

16. Kasas S, Thomson NH, Smith BL, Hansma PK, Miklossy J, Hansma HG (1997) Biological applications of the AFM: From single molecules to organs. International Journal of Imaging Systems and Technology 8 (2):151-161. doi:https://doi.org/10.1002/(SICI)1098-1098(1997)8:2<151::AID-IMA2>3.0.CO;2-9

17. Stylianou A (2017) Atomic Force Microscopy for Collagen-Based Nanobiomaterials. Journal of Nanomaterials 2017 (1):9234627. doi:https://doi.org/10.1155/2017/9234627

18. Allison DP, Mortensen NP, Sullivan CJ, Doktycz MJ (2010) Atomic force microscopy of biological samples. WIREs Nanomedicine and Nanobiotechnology 2 (6):618-634. doi:https://doi.org/10.1002/wnan.104

19. Andriotis OG, Nalbach M, Thurner PJ (2023) Mechanics of isolated individual collagen fibrils. Acta Biomaterialia 163:35-49. doi:https://doi.org/10.1016/j.actbio.2022.12.008

20. Blank RD, Boskey AL (2008) Genetic Collagen Diseases: Influence of Collagen Mutationson Structure and Mechanical Behavior. In: Fratzl P (ed) Collagen: Structure and Mechanics. Springer US, Boston, MA, pp 447-474. doi:10.1007/978-0-387-73906-9_16

21. Yamauchi M, Sricholpech M (2012) Lysine post-translational modifications of collagen. Essays in Biochemistry 52:113-133. doi:10.1042/bse0520113

22. Stammers M, Ivanova IM, Niewczas IS, Segonds-Pichon A, Streeter M, Spiegel DA, Clark J (2020) Age-related changes in the physical properties, cross-linking, and glycation of collagen from mouse tail tendon. Journal of Biological Chemistry 295 (31):10562-10571. doi:10.1074/jbc.RA119.011031

23. Snedeker JG, Gautieri A (2014) The role of collagen crosslinks in ageing and diabetes - the good, the bad, and the ugly. Muscles, ligaments and tendons journal 4 (3):303-308

24. Winkler J, Abisoye-Ogunniyan A, Metcalf KJ, Werb Z (2020) Concepts of extracellular matrix remodelling in tumour progression and metastasis. Nature Communications 11 (1):5120. doi:10.1038/s41467-020-18794-x

25. Hansma HG, Hoh JH (1994) Biomolecular Imaging with the Atomic Force Microscope. Annual Review of Biophysics and Biomolecular Structure 23 (1):115-140. doi:10.1146/annurev.bb.23.060194.000555

26. Kreplak L (2016) Introduction to Atomic Force Microscopy (AFM) in Biology. In: Current Protocols in Protein Science. John Wiley & Sons, Inc. doi:10.1002/cpps.14

27. Main KHS, Provan JI, Haynes PJ, Wells G, Hartley JA, Pyne ALB (2021) Atomic force microscopy—A tool for structural and translational DNA research. APL Bioengineering 5 (3):031504. doi:10.1063/5.0054294

28. Rezaei N, Lyons A, Forde NR (2018) Environmentally Controlled Curvature of Single Collagen Proteins. Biophysical Journal 115 (8):1457-1469. doi:https://doi.org/10.1016/j.bpj.2018.09.003

29. Schneider M, Al-Shaer A, Forde NR (2021) AutoSmarTrace: Automated chain tracing and flexibility analysis of biological filaments. Biophysical Journal 120 (13):2599-2608. doi:https://doi.org/10.1016/j.bpj.2021.05.011

30. Al-Shaer A, Lyons A, Ishikawa Y, Hudson BG, Boudko SP, Forde NR (2021) Sequence-dependent mechanics of collagen reflect its structural and functional organization. Biophysical Journal 120 (18):4013-4028. doi:https://doi.org/10.1016/j.bpj.2021.08.013

31. Al-Shaer A, Forde NR (2024) Decoding Collagen's Thermally Induced Unfolding and Refolding Pathways. bioRxiv:2024.2010.2002.616390. doi:10.1101/2024.10.02.616390

32. Al-Shaer A (2024) Sequence-Dependent Analysis of Collagen's Mechanics and Thermal Stability. Simon Fraser University, Burnaby, BC, Canada

33. Sloseris D, Forde NR (2025) AGEing of collagen: The effects of glycation on collagen's stability, mechanics and assembly. Matrix Biology 135:153-160. doi:https://doi.org/10.1016/j.matbio.2024.12.007

34. Shayegan M, Altindal T, Kiefl E, Forde NR (2016) Intact Telopeptides Enhance Interactions between Collagens. Biophysical Journal 111 (11):2404-2416. doi:10.1016/j.bpj.2016.10.039

35. Stylianou A (2022) Assessing Collagen D-Band Periodicity with Atomic Force Microscopy. Materials 15 (4):1608

36. Mesquida P, Kohl D, Andriotis OG, Thurner PJ, Duer M, Bansode S, Schitter G (2018) Evaluation of surface charge shift of collagen fibrils exposed to glutaraldehyde. Scientific Reports 8 (1):10126. doi:10.1038/s41598-018-28293-1

37. Bansode S, Bashtanova U, Li R, Clark J, Müller KH, Puszkarska A, Goldberga I, Chetwood HH, Reid DG, Colwell LJ, Skepper JN, Shanahan CM, Schitter G, Mesquida P, Duer MJ (2020)

Glycation changes molecular organization and charge distribution in type I collagen fibrils. Scientific Reports 10 (1):3397. doi:10.1038/s41598-020-60250-9

38. Mull V, Kreplak L (2022) Adhesion force microscopy is sensitive to the charge distribution at the surface of single collagen fibrils. Nanoscale Advances 4 (22):4829-4837. doi:10.1039/d2na00514j

39. Wenger MPE, Bozec L, Horton MA, Mesquida P (2007) Mechanical Properties of Collagen Fibrils. Biophysical Journal 93 (4):1255-1263. doi:10.1529/biophysj.106.103192

40. Grant CA, Brockwell DJ, Radford SE, Thomson NH (2009) Tuning the Elastic Modulus of Hydrated Collagen Fibrils. Biophysical Journal 97 (11):2985-2992. doi:10.1016/j.bpj.2009.09.010

41. Grant CA, Phillips MA, Thomson NH (2012) Dynamic mechanical analysis of collagen fibrils at the nanoscale. Journal of the Mechanical Behavior of Biomedical Materials 5 (1):165-170. doi:https://doi.org/10.1016/j.jmbbm.2011.08.020

42. Baldwin Samuel J, Quigley Andrew S, Clegg C, Kreplak L (2014) Nanomechanical Mapping of Hydrated Rat Tail Tendon Collagen I Fibrils. Biophysical Journal 107 (8):1794-1801. doi:10.1016/j.bpj.2014.09.003

43. Pang X, Lin L, Tang B (2017) Unraveling the role of Calcium ions in the mechanical properties of individual collagen fibrils. Scientific Reports 7 (1):46042. doi:10.1038/srep46042

44. Andriotis OG, Elsayad K, Smart DE, Nalbach M, Davies DE, Thurner PJ (2019) Hydration and nanomechanical changes in collagen fibrils bearing advanced glycation end-products. Biomed Opt Express 10 (4):1841-1855. doi:10.1364/boe.10.001841

45. Baldwin SJ, Sampson J, Peacock CJ, Martin ML, Veres SP, Lee JM, Kreplak L (2020) A new longitudinal variation in the structure of collagen fibrils and its relationship to locations of mechanical damage susceptibility. Journal of the Mechanical Behavior of Biomedical Materials 110:103849. doi:https://doi.org/10.1016/j.jmbbm.2020.103849

46. Cisneros DA, Hung C, Franz CM, Muller DJ (2006) Observing growth steps of collagen self-assembly by time-lapse high-resolution atomic force microscopy. Journal of Structural Biology 154 (3):232-245. doi:https://doi.org/10.1016/j.jsb.2006.02.006

47. Gisbert VG, Benaglia S, Uhlig MR, Proksch R, Garcia R (2021) High-Speed Nanomechanical Mapping of the Early Stages of Collagen Growth by Bimodal Force Microscopy. ACS Nano 15 (1):1850-1857. doi:10.1021/acsnano.0c10159

48. Roth J, Hoop C, Williams JK, Nanda V, Baum J (2024) Real-time single-molecule observation of incipient collagen fibrillogenesis and remodeling. Proceedings of the National Academy of Sciences 121 (33):e2401133121. doi:doi:10.1073/pnas.2401133121

49. Shayegan M, Forde NR (2013) Microrheological Characterization of Collagen Systems: From Molecular Solutions to Fibrillar Gels. PLOS ONE 8 (8):e70590. doi:10.1371/journal.pone.0070590

50. Rezaei N (2016) Mechanical Studies of Single Collagen Molecules Using Imaging and Force Spectroscopy. PhD Thesis, Simon Fraser University, Burnaby, BC, Canada

51. Rivetti C, Guthold M, Bustamante C (1996) Scanning Force Microscopy of DNA Deposited onto Mica: Equilibration versus Kinetic Trapping Studied by Statistical Polymer Chain Analysis. Journal of Molecular Biology 264 (5):919-932. doi:http://dx.doi.org/10.1006/jmbi.1996.0687

52. SmarTrace. https://github.com/FordeLab/SmarTrace.

53. DipLib. https://github.com/DIPlib/diplib.

54. Li Y, Asadi A, Monroe MR, Douglas EP (2009) pH effects on collagen fibrillogenesis in vitro: Electrostatic interactions and phosphate binding. Materials Science and Engineering: C 29 (5):1643-1649. doi:https://doi.org/10.1016/j.msec.2009.01.001

55. Morozova S, Muthukumar M (2018) Electrostatic effects in collagen fibril formation. The Journal of Chemical Physics 149 (16). doi:10.1063/1.5036526

56. Darvish DM (2022) Collagen fibril formation in vitro: From origin to opportunities. Materials Today Bio 15:100322. doi:https://doi.org/10.1016/j.mtbio.2022.100322

57. Wieczorek A, Rezaei N, Chan CK, Xu C, Panwar P, Brömme D, Merschrod S EF, Forde NR (2015) Development and characterization of a eukaryotic expression system for human type II procollagen. BMC Biotechnology 15 (1):112. doi:10.1186/s12896-015-0228-7

58. Wieczorek A, Chan CK, Kovacic S, Li C, Dierks T, Forde NR (2018) Genetically modified human type II collagen for N- and C-terminal covalent tagging. Canadian Journal of Chemistry 96 (2):204-211. doi:10.1139/cjc-2017-0335

59. Kowalewski A, Forde NR (2024) Fluence-dependent degradation of fibrillar type I collagen by 222 nm far-UVC radiation. PLOS ONE 19 (1):e0292298. doi:10.1371/journal.pone.0292298

Table 1. Key parameters and relations for describing polymer flexibility using the standard WLC model in two dimensions (as for polymers on a surface).

Parameter, symbol	Definition	Equation
Contour Length, L	The length along the entire backbone of a polymer.	
Segment length, s	A length along a shorter stretch of the polymer's backbone.	
Persistence Length, p	A measure of the flexibility of a polymer, representing the length over which the chain directionality decorrelates. Shorter persistence lengths reflect more flexible polymers.	$p = \kappa/k_B T$, where κ is the bending stiffness of the polymer, k_B is the Boltzmann constant, and *T* is temperature in Kelvin
Mean Squared End-to-End Distance, $\langle R^2(s) \rangle$	The average square of the through-space distance between the two points along a polymer separated by a distance s along its backbone.	$\langle R^2(s) \rangle = 4ps \left(1 - \frac{2p}{s}\left(1 - e^{-\frac{s}{2p}}\right)\right)$
Tangent Vector Correlation, $\langle cos\ \theta(s) \rangle$	The average cosine of the angle between two tangent vectors separated by a distance s along the polymer's backbone.	$\langle cos\ \theta(s) \rangle = e^{-\frac{s}{2p}}$

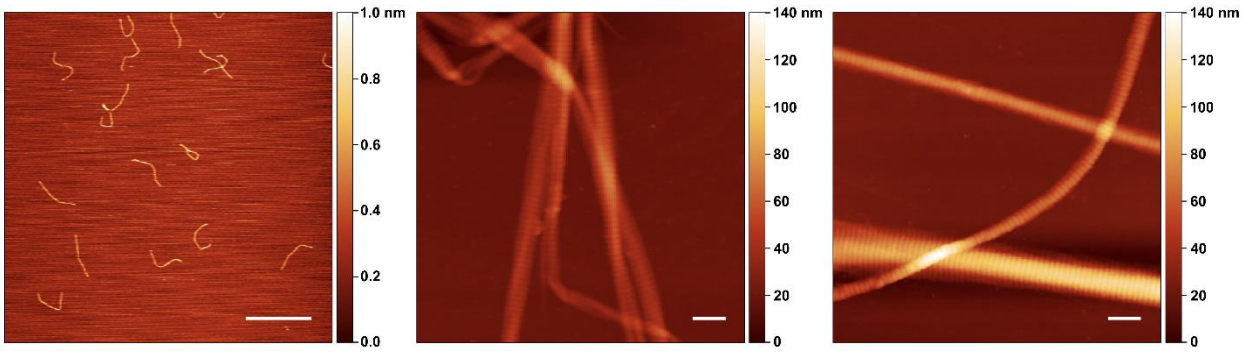

Figure 1. Atomic force microscopy images of type I collagen. Individual collagen proteins deposited from 10 mM KCl, 1 mM HCl at pH 3.0 (left), reconstituted collagen fibrils deposited from 1X fibril-forming buffer at pH 7.0 (middle), and tendon-extracted collagen fibrils deposited from PBS (right). Scale bars = 400 nm.

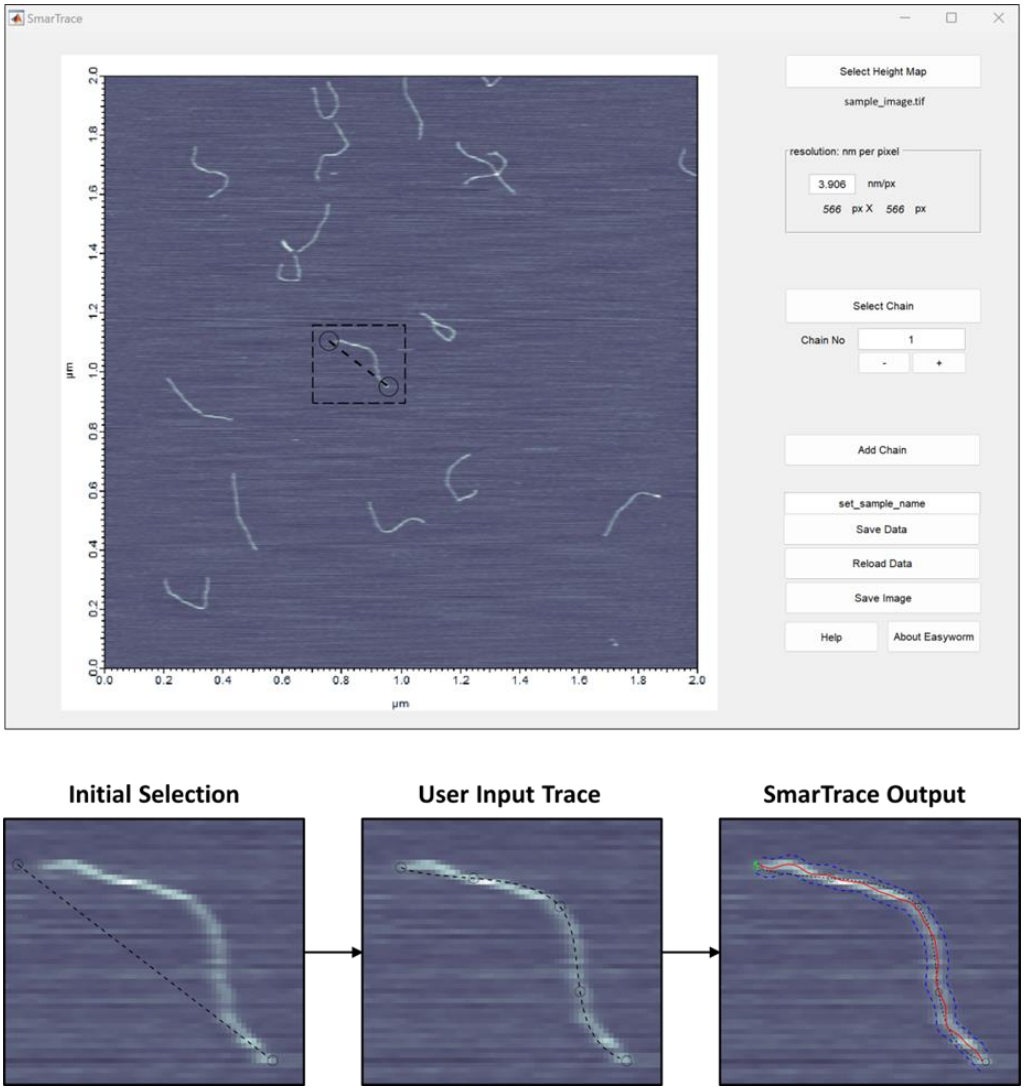

Figure 2. The SmarTrace GUI window. Use the Select Height Map button to open images containing the chains to be analysed. The resolution (nm per pixel) should be defined before tracing. To begin, press the Select Chain button and select at least two points along the chain of interest, then press 'Z' to zoom in. Press 'D' to delete the initial selection and retrace the chain with better precision, then press Enter. The refined spline, output by SmarTrace, is displayed in red, while the dashed lines represent the width of the chain, which is used to determine the path of the backbone but is not used for subsequent analysis with the WLC model.

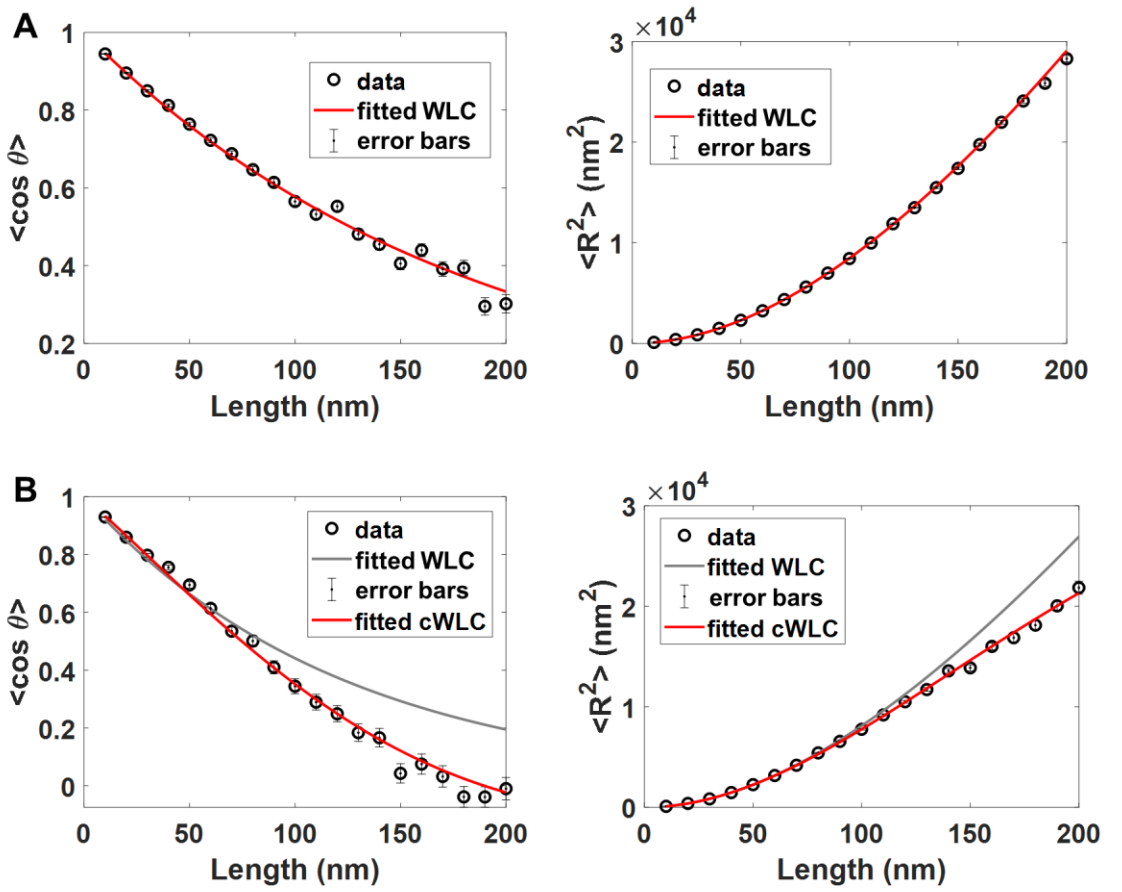

Figure 3: Worm-like chain model fits from SmarTrace output folder. A. Type I collagen, deposited from 100 mM KCl and 1 mM HCl (pH 3.0), is well described by the standard WLC model. *N* = 441 chains. **B.** Type I collagen, deposited from 10 mM KCl and 1 mM HCl (pH 3.0), is not well described by the standard WLC model, but is better characterized by the curved WLC model (cWLC). *N* = 104 chains.

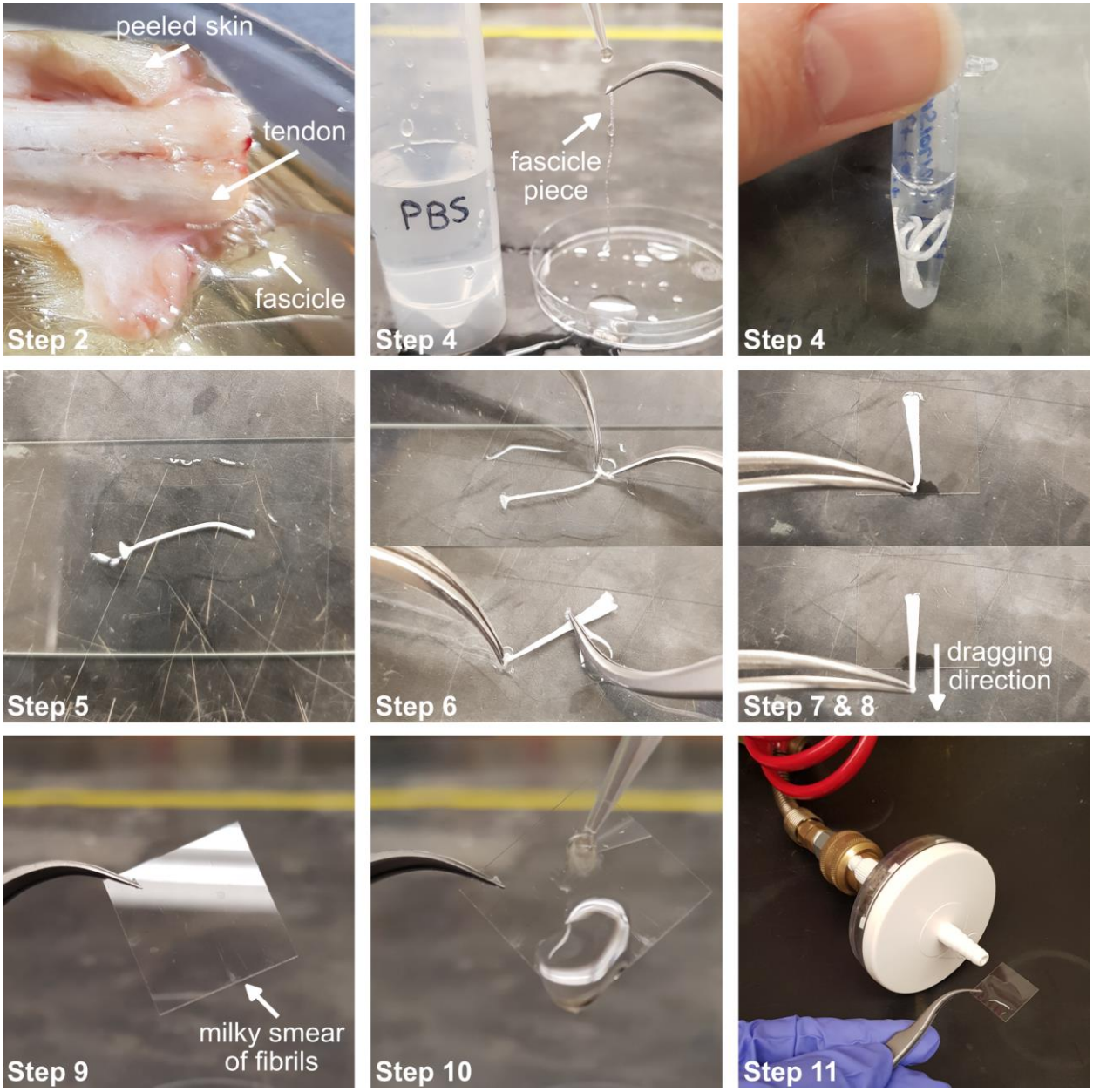

Figure 4. Tendon extraction and sample preparation. Depiction of select steps for extracting tendons from rat tails and streaking them across a glass surface to immobilize individual collagen fibrils for AFM imaging.